The electro-dynamics of the dendritic space in Purkinje cells of the cerebellum.

Irina B. Kulagina * Sergey M. Korogod *

Ginette Horcholle-Bossavit † Cesira Batini ‡

Suzanne Tyč-Dumont †

Corresponding author: **Ginette Horcholle-Bossavit**†

Running title: dendritic spatial dynamics

Keywords: Dendritic geometry - Purkinje neurons - oscillatory potentials - spatio-temporal patterns - electro-geometrical coupling

*International Center for Molecular Physiology (Dniepropetrovsk Division), National Academy of Sciences of Ukraine 49050 Dniepropetrovsk, Ukraine.

†UMR-CNRS 7084-SOMA. Laboratoire d'Électronique, ESPCI, 10 rue Vauquelin, 75005 Paris, France. Tel/Fax: 33 1 40 79 44 64, e-mail: ginette.bossavit@espci.fr

‡Laboratoire de Génétique Moléculaire de la Neurotransmission et des Processus Neurodégénératifs, Université Pierre et Marie Curie, UMR7091-CNRS, 75013 Paris, France.

abstract

The functional geometry of the reconstructed dendritic arborization of Purkinje neurons is the object of this work. The combined effects of the local geometry of the dendritic branches and of the membrane mechanisms are computed in passive configuration to obtain the electrotonic structure of the arborization. Steady-currents applied to the soma and expressed as a function of the path distance from the soma form different clusters of profiles in which dendritic branches are similar in voltages and current transfer effectiveness. The locations of the different clusters are mapped on the dendrograms and 3D representations of the arborization. It reveals the presence of different spatial dendritic sectors clearly separated in 3D space that shape the arborization in ordered electrical domains, each with similar passive charge transfer efficiencies. Further simulations are performed in active configuration with a realistic cocktail of conductances to find out whether similar spatial domains found in the passive model also characterize the active dendritic arborization. During tonic activation of excitatory synaptic inputs homogeneously distributed over the whole arborization, the Purkinje cell generates regular oscillatory potentials. The temporal patterns of the electrical oscillations induce similar spatial sectors in the arborization as those observed in the passive electrotonic structure. By taking a video of the dendritic maps of the membrane potentials during a single oscillation, we demonstrate that the functional dendritic field of a Purkinje neuron displays dynamic changes which occur in the spatial distribution of membrane potentials in the course of the oscillation. We conclude that the branching pattern of the arborization explains such continuous reconfiguration and discuss its functional implications.

INTRODUCTION

The Purkinje neuron is a peculiar cell in the central nervous system. Besides the fact that its isoplanar anatomical organization has been conserved throughout evolution (14; 37), the cerebellar Purkinje cell with its single dendrite is the only output of the cerebellar cortex, making it a chief card for understanding the cerebellar function. This cell has been extensively studied for decades. Its morphology, its physiology and the underlying mechanisms are well documented (15; 18; 14; 5; 27; 28; 45). Considerable information is available concerning the intracellular response properties of the Purkinje cell and its connectivity and functions. Since the first description that depolarization of the Purkinje cell by intracellular injected currents *in vitro* evokes Na^+ dependent somatic spikes and Ca^{++} dependent dendritic spikes (39; 40), it is well known that spontaneous firing of the Purkinje cell is characterized by burst-like activity consisting of both somatic spikes and dendritic depolarizing spikes. In the cerebellar slice preparation, Purkinje cell fire dendritic spikes in burst under certain conditions such as depolarization or a decrease in extracellular Na^+ concentration (29; 3). Results obtained from experiments in which the effects of tetrodotoxine (TTX) were observed both *in vitro* and *in vivo* and for both intact Purkinje cells and in Purkinje cells deprived of their climbing fibers, show that TTX suppresses the somatic spikes within a few seconds and the dendritic spikes then appeared grouped into bursts (3). TTX addition to the bath left the basic spontaneous activity and its frequency unaltered indicating that Ca^{++} spiking and Ca^{++} dependent K conductance changes are the main events underlying the oscillatory behaviour. Further experiments demonstrated that Purkinje oscillatory activity was modulated by $GABA_B$ receptors in the dendrites and $GABA_A$ receptors in the soma and dendrites (64; 65). Moreover, bistability of Purkinje neurons has been analyzed in details by (67) and by (41).

The aim of our simulation study is to describe precisely the membrane potentials that

characterize the whole dendritic arborization when the Purkinje neuron generates these oscillatory potentials known to exist in these neurons. The features of the Purkinje cell discharges are expressed by the local electrical states of any dendritic sites determined by the currents that flow between any sites and to and from the soma during transients. These spatial features are not yet fully described and are not yet explained in terms of the combined effects of the membrane mechanisms and the local geometry of the dendritic branches.

In addition to other Purkinje cell models previously published in the literature (50; 51; 11; 12; 53; 63; 67; 41) which replicate the features of the Purkinje cell discharges recorded from live neurons, we propose here to focus our simulations on the analysis of the spatial electrical patterns of the dendritic membrane, explored under passive and active conditions. We implement a model of Purkinje neuron in which the fast discharge mechanisms are deliberately excluded to cast light only on the spatial patterns of the slow oscillatory activity in the whole dendritic arborization. This reductive approach provides the electrical dynamics of the whole dendritic space that can only be computed and cannot be recorded from live cells yet.

The electrotonic structure of the passive dendrite provides a basic reference for understanding how geometry plays a crucial role in determining dendritic processing of the neuron (6; 7). In previous studies, we have shown the prominent impact of dendritic geometry on somatopetal transfer of the current generated by steady uniform activation of excitatory synaptic conductances distributed over passive dendrites. By using different values of specific membrane resistivity and assuming that the membrane conductivity $G_m = 1/R_m$ was an approximately linear function of the input firing rate, we mimicked high and low pre-synaptic activities (31; 35; 34). When expressed by the somatopetal current transfer effectiveness as a function of the physical distance from the soma (4; 8; 35), it contains unique information on the geometrical features that

rule the transfer effectiveness of the dendrite. Namely, in a theoretical work, we have demonstrated that electrical differences between the dendritic path profiles could only occur because of differences in length and diameters between daughter branches along the dendritic paths in the whole arborization (35). These two metrical parameters define the **metrical asymmetry** of the dendritic branching. This notion helps to interpret further our findings in non-linear conditions.

Our simulation tools provide maps of the spatial distribution of membrane potentials over the passive Purkinje cell dendrite and when the active Purkinje cell generates slow oscillatory potentials. Under both conditions, we show that the dendritic arborization is similarly partitioned into several spatial sectors of different effectiveness, the electrical states of which are ordered in a given geometry-related manner. We demonstrate that metrical asymmetry of the dendritic branches is responsible for such spatial partitions in effectiveness. Finally, to verify the robustness of our findings, we test with the same simulation protocol, the responses of five other Purkinje neurons reconstructed and analyzed in other laboratories (51; 53). We find similar spatial partitions of the dendritic arborization, both in the steady state and during oscillatory activity in all cells. We conclude that such compartmentalization is a general rule for the arborization of the Purkinje neuron. Our findings is related to the key role of dendritic geometry and suggest that the neuron output pattern in terms of action potentials initiation sites must be revisited.

MATERIAL and METHODS

The Purkinje cell (P1) fully analyzed in this work was selected from a series of intracellularly labelled Purkinje cells studied in slices of rat cerebellum. Methods of surgical preparations, electrophysiological recordings, intracellular staining and histological procedures were described in details by (64; 65). This cell was reconstructed at high spatial

resolution with a three dimensional computer-aided system in our laboratory by one operator (GHB). The procedure for data acquisition has been described previously in detail in (6) and (34). Briefly, the labelled neuron was observed using a microscope (Orthoplan; Leitz, Wetzlar, Germany) with a $0.1\mu m$ XY resolution motorized stage (EK 32; Maertzhauser) and microprocessor interface (Lang Electronics) with a Leitz plan x100/1.25 NA oil immersion objective lens at a final magnification of 1,250. A stepping motor controlled the focus in Z direction at a resolution of 0.1μm. The dendritic segments were described by a series of data points separated by a 3D distance with a controlled sampling interval ranging from 0.5μm to 10μm. The diameter of the profile was measured at 0.2μm resolution using a circle displayed on an oscilloscope and adjusted to the profile. A new data point was entered whenever a change in diameter was observed. Each point was identified by 6 parameters: sequential number; x, y, z coordinates; diameter of the profile; topological identifier. The computer-microscope system was implemented by P. Gogan (6) on the basic principle described by (16) and (66). A shrinking coefficient of the cell in slices was not calculated. At the end, the dendritic arborization of P1 was stored in a data base together with fiducial marks. A dedicated software program was used for computer reconstruction of the arborization.

The five other Purkinje neurons analyzed in this work were retrieved from the works of (51; 53). They were posted in ModelDB

($http://senselab.med.yale.edu/senselab/modeldb/$) and downloaded from

($http://www.dendrite.org/dendritica-1.0/batchback/data/cells$) in the files importable into NEURON simulation software (21; 20). Two Purkinje cells from (53): P19.hoc (368K) named P2 in this work and P20.hoc (196K) named P3 and three Purkinje cells from (51): cell1, (240K) named P4, cell2, named P5 (265K) and cell3, (364K) named P6.

NEURON simulator (21; 20) was used for computation.

Neuron model

The constructed model was built with a cylinder-shaped soma of $20\mu m$ length, and $22.5\mu m$ diameter, an initial segment of $20\mu m$ length and $5\mu m$ diameter, a stem axon of $200\mu m$ length with a $3\mu m$ diameter and the numerized dendritic arborization of the Purkinje cell. Dendritic spines were not reconstructed. However, the dendritic branches were classified as smooth or spiny according to their Strahler orders and their diameter (58). It was assumed that in Purkinje cells, transition from spiny to smooth dendrites occurred at branches of fourth Strahler order (23; 27). Therefore, we classified a branch as spiny if it had a Strahler order exceeding four or if its diameter was thinner than $2\mu m$. With these two criteria in our initial classification, only 55 of the total 539 branches mismatched. Further careful consideration of the morphology resulted in classifying these ambiguous branches as 23 smooth and 32 spiny branches. Then, the ultimate classification was 56 smooth and 483 spiny dendritic branches.

Simulated membrane properties

The same reconstructed Purkinje cell structure was used for computing the electrical states of the whole arborization under passive and active conditions. The specific membrane capacitance C_m was 0.8 for the soma and 1 $\mu F/cm^2$ for the axon.

The passive model

In all simulations, the soma and axon were passive with membrane conductivity G_m = 667.25 $\mu S/cm^2$ and a reversal potential E_p = -65 mV. The specific membrane capacitance C_m = 1 $\mu F/cm^2$ and the cytoplasmic resistivity R_i = 250 Ωcm were homogeneous throughout the dendrite. These values were taken from earlier models of Purkinje neurons (51; 11; 48). The passive specific membrane conductance G_m was spatially homogeneous and tested with values from 10 to 10,000 $\mu S/cm^2$ simulating different levels

of tonic activation homogeneously distributed over the dendritic surface. Within this range, two values (G_m = 40 and 350 $\mu S/cm^2$) were selected for illustrating the effects of low and high synaptic activation on the spatial distribution of the membrane voltage (Fig 3). As in our previous works (31; 34), the electrotonic structure of the cell was represented by profiles of the relative charge transfer effectiveness $T(x)$ as a function of the path distance x from the soma estimated as in (4). To obtain $T(x)$, we computed the steady transmembrane voltage distribution $E(x)$ over the whole arborization in response to a direct steady current applied to the soma. The current intensity was adjusted to get 10 mV deviation of the voltage $E(0)$ at the somatic end of the dendrite (x = 0) from the resting potential of the passive membrane E_p. We used the known directional reciprocity of the somatofugal attenuation of voltage and the somatopetal attenuation of current (8; 35) to calculate the path distribution of the charge transfer as $T(x) = (E(x) - E_p)/(E(0) - E_p)$.

To test the validity of the results obtained on P1, we used the morphologies of other Purkinje neurons described by (51) and (53).

The active model

The specific cytoplasm resistance was R_i =250 Ωcm (51) throughout the cell. The soma and axon were passive with membrane conductivity G_m = 667.25 $\mu S/cm^2$, G_m = 6672.5 $\mu S/cm^2$, G_m = 66,725 $\mu S/cm^2$ and a reversal potential E_p = -65 mV. To take into account the contribution of spines to the membrane area (4.4 spines per 1 μm dendritic length, each spine having a membrane area 1.1 μm^2, as in (58)), the membrane capacitance was set to =1.5 $\mu F/cm^2$ for the spiny branchlets whereas it was set to 0.8 $\mu F/cm^2$ for the soma and smooth, non-spiny dendritic branches as described in the model implemented by (48). Tonic activation of excitatory synaptic inputs (AMPA type) distributed over the whole arborization was simulated by introducing homogeneous voltage-independent synaptic conductance G_s = 100 $\mu S/cm^2$ and reversal potential E_s

$= 0mV$ in the dendritic membrane.

The same set of ion channels as described by others (48; 11; 12) was incorporated in the reconstructed dendritic arborization of our model. Since our study focused on slow oscillatory potentials, we tested which channels could be excluded from the original set without affecting the slow oscillatory pattern. After the test, an ultimate set of dendritic channels was defined: the P-type calcium (CaP) (38), delayed rectifier potassium (Kdr)(68), A-type potassium (KA)(22), high-threshold Ca-activated potassium (KC) currents (36) and the passive leak current (I leak). Other channels were not included in our model because they conducted ions with one or two order lower conductance (T- and E-type calcium currents; the D-type, persistent, and low threshold Ca-activated potassium currents) or because they were not involved in shaping the oscillatory potentials but in shaping the spikes at soma (fast and persistent sodium currents and anomalous rectifier potassium current). Unlike the reference models (48; 11; 12), the fast discharge mechanisms were excluded from our model because we focused on spatial electrical pattern during the slow oscillations and not during action potentials.

The choice of the colour-coded scales

First, we computed the distribution of voltage along all paths of the arborization and plotted it as a function of the path distance from the soma which is the common root of all paths (see Fig.3) A, C. The branching multi-path plot was topologically equivalent (homeomorphous) to the morphological arborization. It had the same number of connected branches and paths as the neuronal dendrites. Hence, we obtained an electrical image of the arborization represented by the corresponding tree of the path distance profiles of voltages. The more similar the voltages along different branches and paths were, the closer the path profiles of voltages on the multi-path plot were. Bundles of closely running path profiles corresponded to groups of branches and paths showing similar electrical state. An algorithm of the code of colours was implemented in order

to identify the location of the dendritic domains which have similar electrical states. We use colour to illustrate the location of the bundles of similar voltage profiles on the dendrograms and the 3D representations of the arborization. Arbitrarily, we chose six colours to code the voltages and applied the colour-coded scale to all spatial representations. We adjusted the colour-coded scale to the voltage range enveloping a cluster of profiles so that the branches in the cluster had the same colour, thus setting the voltage limits for each color of the scale.

RESULTS

The quantitative geometry of the Purkinje cell

The reconstructed dendritic arborization of P1 (Fig.1A and B) was described by 3,484 data points. Typically, the single stem dendrite divided into secondary branches giving rise to 539 dendritic segments. The total length of all dendritic segments was 6,765 μm and the total dendritic surface area was 24,041 μm^2. The quality of the morphological description was checked by analyzing the 3D sampling interval (24; 30). The distribution of the sampling intervals showed a peak at $1.5\mu m$, indicating the most frequently used sampling interval and a smooth frequency distribution (Fig. 1C). As the diameter sampling was also indicative of the quality of the reconstruction, it was analyzed by plotting the frequency distribution of the diameter of all data points using a bin width smaller than or equal to half the minimum measurable diameter to avoid aliasing effects (Fig. 1D). It was smooth without holes and the most frequently measured diameter was around 0.5 μm . These two observations attested a correct reconstruction at high spatial resolution.

To assess the reliability of the model, we used five Purkinje cells retrieved from (51) and (53) and compared the results obtained with our reconstructed cell P1 to those

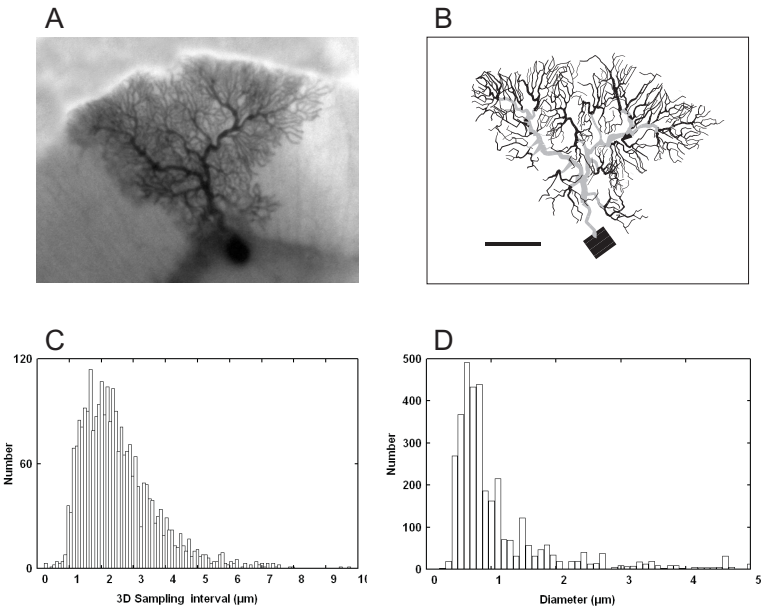

Figure 1: Quantitative geometry of the Purkinje cell. **A**: photomicrograph of the labelled Purkinje cell in a rat cerebellar slice. **B**: two dimensional representation of the Purkinje cell reconstructed at high spatial resolution. The 56 smooth dendritic branches are indicated in grey and the 483 spiny dendritic branches are in black. Calibration bar = 50 μm. **C**: sampling accuracy: analysis of the three-dimensional sampling intervals. The distribution is built using a bin width of 0.2 μm and clip to values less than 10 μm. **D**: histogram of the diameter distribution built with a bin width of 0.1 μm.

.

produced by the other slightly different morphologies. As the diameter is one of the indicators of quality of the reconstruction and its inequality contributed to the metrical asymmetry of dendritic branches, an analysis of the distribution of the diameters as a function of the path distance was performed for each Purkinje neuron (Fig. 2). The main finding was some difference between cells in the diameters of the dendritic tips. P1 displayed smaller and more homogeneous tip diameters than the five other Purkinje cells which displayed larger and more scattered tip diameters.

The same accurate quantitative morphology of P1 was used to simulate the electrical states of the dendritic membrane when the arborization was a passive electrical skeleton and when active membrane conductances were incorporated into the model. Thus, the simulation experiments shared an identical dendritic geometry and differed only by their

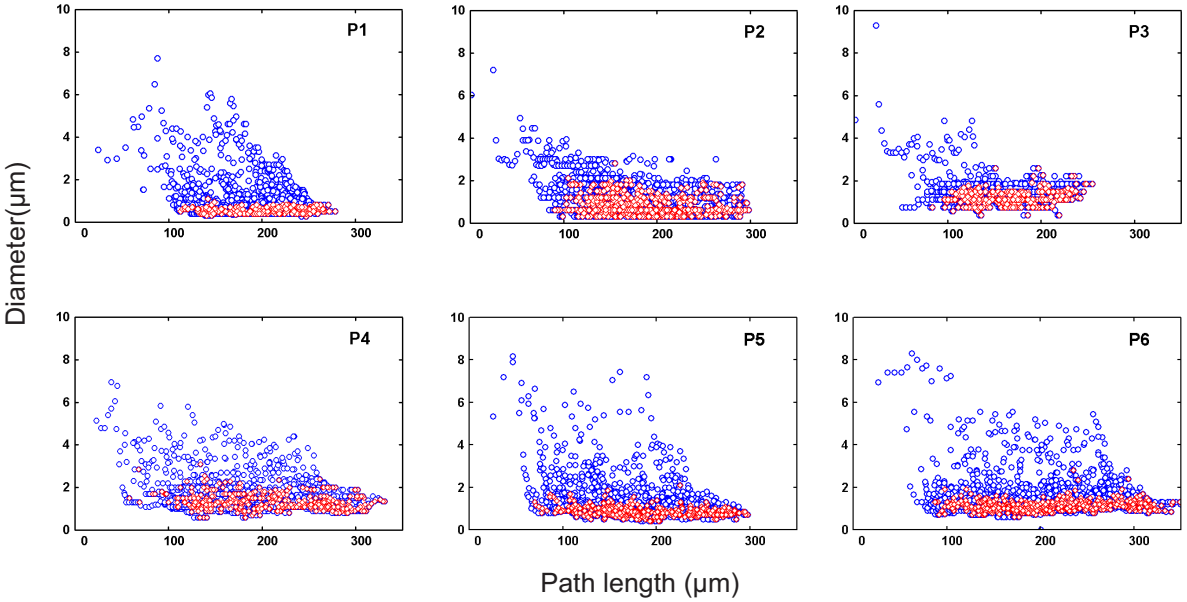

Figure 2: Analysis of the distribution of the dendritic diameters in the six Purkinje cells P1 to P6 identified in Material and Methods. Diameters in μm (ordinates) as a function of path distance from the soma in μm(abcissae).White circles: values of all measured diameters; black circles: values of diameters for terminal segments.

.

membrane electrical properties. We next compared the results of this simulation with those performed on the five other Purkinje neurons under passive conditions.

The passive configuration

As no mathematical tool was available to obtain a quantitative description of metrical asymmetry of dendritic branches, we used the electrotonic structure of the arborization as the best indirect indicator for revealing metrical asymmetry of dendritic paths (7; 31; 35). The spatial profiles of somatofugal voltages are equivalent to the somatopetal current transfer effectiveness plotted as function of the path distance from the soma (4; 8; 35). The electrotonic structure of the arborization was computed under two different uniform specific membrane resistance of 25.0 and 2.86 $k\Omega cm^2$. Correspondingly, the somatopetal current transfer effectiveness $T(x)$ of the whole passive dendritic arborization was obtained under two conditions of homogeneous tonic synaptic activation

by setting the specific membrane conductance G_m at a low (40 $\mu S/cm^2$) and high value (350 $\mu S/cm^2$).

The results of these computations are shown in Fig. 3 in which the distribution of $T(x)$ along all dendritic paths represented the electrotonic structure of the arborization (Fig. 3A, C). Since each profile of the plot represented the current transfer effectiveness along a given dendritic branch, the branching plot of $T(x)$ was topologically homeomorphous to the reconstructed dendritic arborization. When the distribution of electrotonic potentials along the dendritic arborization in the spatial domain was expressed, a diversity of heterogeneous electrotonic properties was observed. As expected, $T(x)$ decreased with path distance from the soma. The decay was smooth along uniform segments and sloped down at the sites of abrupt changes in diameter or asymmetrical branching as already demonstrated in previous works (7; 31; 35; 34). The structure of the whole arborization displayed bundles of profiles that were more or less compacted according to the values of G_m. It was checked that whatever G_m from 10 to 10,000 $\mu S/cm^2$, the presence of bundles with similar $T(x)$ was preserved although the absolute values of electrotonic potentials were modified. For example in Fig. 3 A, at low synaptic activation (G_m = 40 $\mu S/cm^2$), the profiles were compacted and displayed similar $T(x)$ between 0.8 and 1. However, two slightly divergent bundles of profiles were distinguished, one of them in the longest branches, over 200 μm from soma. In contrast, at high tonic activation (G_m = 350 $\mu S/cm^2$), the $T(x)$ profiles displayed divergent $T(x)$ producing heterogeneous separation of the curves with different gradients indicating different transfer effectiveness of branches situated at similar physical distances from soma (Fig. 3 C). The difference in voltage between some branches was small enough to produce grouping of the branches with similar electrotonic decay. That such grouping might exist in the arborization was demonstrated in a previous work which showed that the electrotonic structure could be reduced to a statistically significant small set of well discriminated

clusters (35). Bundles of profiles which were formed by dendritic branches with similar electrotonic potential could be clearly identified in the 1D representation (green, blue, magenta arrows in Fig. 3 C). The arrows point at three different bundles which are different in their transfer effectiveness, each of them with branches with similar transfer effectiveness. These bundles fully analyzed in our previous works (31; 35; 34; 32) were due to metrical asymmetry between daughter branches.

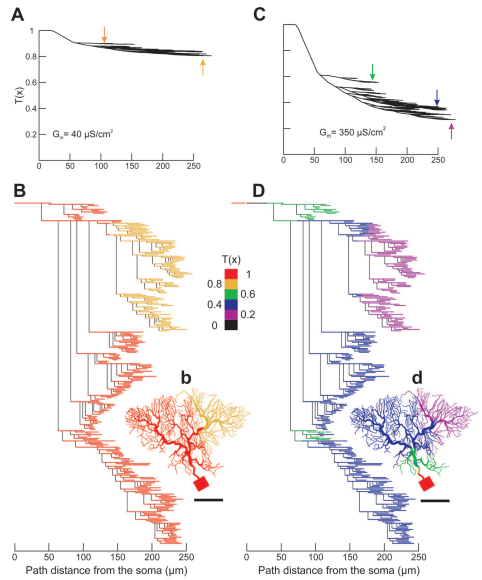

Figure 3: Electrotonic structure of the passive arborization of the Purkinje cell P1. **A and C**: somatopetal charge transfer effectiveness ($T(x)$) is expressed as a function of the path distance x from the soma in μm computed at $G_m = 40\ \mu S/cm^2$ and $G_m = 350\ \mu S/cm^2$. **B and D** : the corresponding dendrograms at low and high G_m painted with the colour-coded values of $T(x)$. **b and d**: Maps of the somatopetal charge transfer effectiveness on the 3D reconstructed Purkinje cell arborization at $G_m = 40\ \mu S/cm^2$ in **b** and $G_m = 350\ \mu S/cm^2$ in **d** as a function of the path distance x from the soma in μm. The arborizations are split into different domains with different $T(x)$. The arrows in **A and C** identify the bundles of profiles by their colours used in dendrograms and 3D representations. Insert: colour-coded $T(x)$ from 0 to 1. Calibration bar: 50 μm.

To localize the bundles with similar transfer effectiveness on the topological (2D) and the 3D representation of the arborization, they were colour-coded by values of $T(x)$ and painted on the dendrograms (Fig. 3 B and D) and the 3D representation of the dendritic field (Fig. 3 b and d). While the dendrograms showed the position of each

branch as a function of the path distance from soma, the 3D representation revealed the spatial location of the branches of a given effectiveness within the dendritic field. At low G_m ($G_m = 40\mu S/cm^2$), the colour-coded maps of the arborization were reduced to only two homogeneous compacted domains with high efficiency ($T(x) = 0.8$ to 1) that occupied two distinct sectors of the dendritic field (Fig. 3 B and b). A large one with $T(x)$ close to 1 involved the main part of the dendritic field from 0 to 250 μm from the soma and a smaller one ($T(x)$ about 0.8) located in the North-East sector of the dendritic field from 130 to 250 μm from the soma. At high G_m, ($G_m = 350\ \mu S/cm^2$), the values of $T(x)$ ranged between 0.2 to 1.0 (Fig. 3 D and d). The most effective ($T(x)$ from 0.8 to 1) concerned only the proximal part of the primary dendrite up to 25 μm from the soma. Followed a region ($T(x) = 0.6$) of small size and low complexity from 25 to 130 μm from the soma, giving rise to a large and most complex domain of the dendritic field with $T(x)$ about 0.4. The least efficient domain was located in the North-East sector of the dendritic field and extended from 150 μm to the tips of the dendritic branchlets. It overlapped with the preceding domain in terms of path distances from soma (dendrogram) but was clearly identified spatially on the 3D representation (Fig. 3 d). The main observation was the specific spatial occupation of the dendritic field by the bundles of dendritic branches identified in the 1D representation. They were clearly separated in 3D space forming ordered electrical domains, each with similar passive transfer properties.

The robustness of the dendritic partitions tested on different Purkinje cell morphologies

To test whether our findings obtained on P1 could be generalized to other Purkinje neurons and were not just incidental to this particular neuron, the same simulation protocol was applied to five other reconstructed Purkinje neurons (P2 to P6) described

in Material and Methods. Their passive electrotonic structures were represented by the path distance profiles of the steady voltage computed with the same parameters as for P1. By inserting the same membrane parameters in each cell, we have isolated the effect of dendritic geometry.

The results of the computations are shown in Fig. 4. The comparison of the six electrotonic structures (plots P1 to P6 in Fig. 4) revealed common features between neurons and some cell-specific features. Similarities were the path profiles grouped together into more or less dense bundles corresponding to sets of paths with similar voltage transfer. The asymmetrical dendritic paths were separated by different voltages but run along each other over path distances of several tens of micrometers indicating that multiple segments were situated equidistantly from soma although characterized by different voltages and thus, different passive transfer properties. The cell-specific voltage features were observed at the most distal dendritic tips which ranged from about -66.5 mV in P5 to -68.5 mV in P2, compared to the same voltage (-60 mV) at the soma. The voltage difference between the tips of the shortest and longest dendritic paths ranged from about 3.5 mV in P1 to about 6 mV in P3, P4, and P6. Finally, the number and mutual position of individual path profiles and their pattern itself were cell-specific.

On the 3D image of the arborizations (inserts in Fig. 4), the dendritic domains with similar (same colour) or dissimilar (different colour) voltages were located in the dendritic fields. We found two main types of partition of the dendritic arborizations. In four cells (P1, P3, P4, and P6), the domains looked like planar sectors approximately limited by radii (dashed lines) emerging from major branching points. In each case one could distinguish sectors of low (L), medium (M), and high (H) depolarization/effectiveness. In the two other cells (P2 and P5), the partition of the whole arborization looked more patchy. The feature of these two arborizations was the presence of two main highly complex sub-trees emerging from two (P5) or three (P2) thick early order branches .

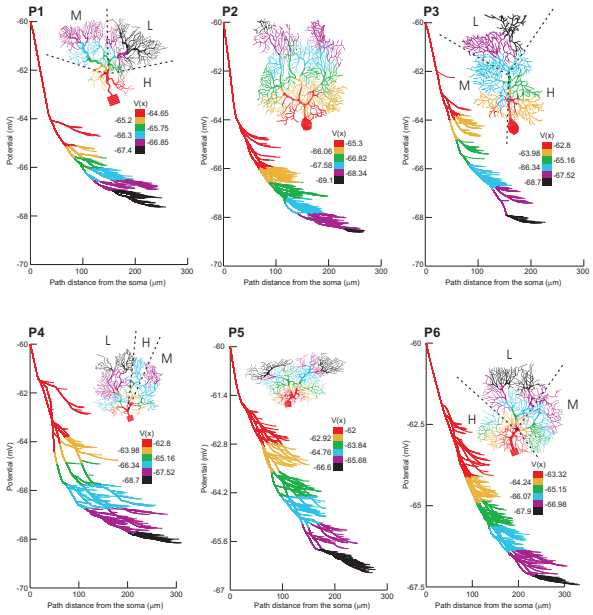

Figure 4: Partition of the dendritic fields into several electrical sectors observed in Purkinje neurons. Electrotonic structures of the passive dendritic arborization of six Purkinje cells, P1 to P6, identified in Material and Methods. For each cell, the voltage along the profiles (ordinates) is expressed in mV as a function of the physical distance x from the soma (abscissae) in μm. The colour-painted profiles indicate voltages according to each colour-scale ($V(x)$) in mV. In insert: the corresponding map of the 3D reconstructed Purkinje neuron, painted with the same colour-scale, to locate the different dendritic sectors characterized by the same voltage. In P1, P3, P4, P6 the domains looked like planar sectors approximately limited by radii (dashed lines) emerging from major branching points. In each case, sectors of low (L), medium (M), and high (H) depolarization/effectiveness are identified. In P2 and P5, the partition of the dendritic fields appears more patchy.

Taken together, these findings demonstrated that dendritic geometry determined the electrical features of the spatial dendritic domains in the six Purkinje neurons.

A realistic model of the active Purkinje neuron arborization

Our simulations were aimed at finding out whether similar spatial domains found in the passive model of P1 also characterized the same dendritic arborization in condition of distributed active conductances. If the regional organization of the electrical space of the dendritic arborization already achieved by the passive structure is also discovered in an active configuration, then our hypothesis of the pivotal role of metrical asymmetry

of dendritic branches will be strongly supported.

A series of simulations were performed in the active configuration with the cocktail of conductances found experimentally in the Purkinje cell arborization during *in vitro* electrical recordings (51; 11; 12; 48). During tonic activation of excitatory synaptic inputs (AMPA type) homogeneously distributed over the whole arborization, the Purkinje cell generated a regular auto-oscillatory activity.

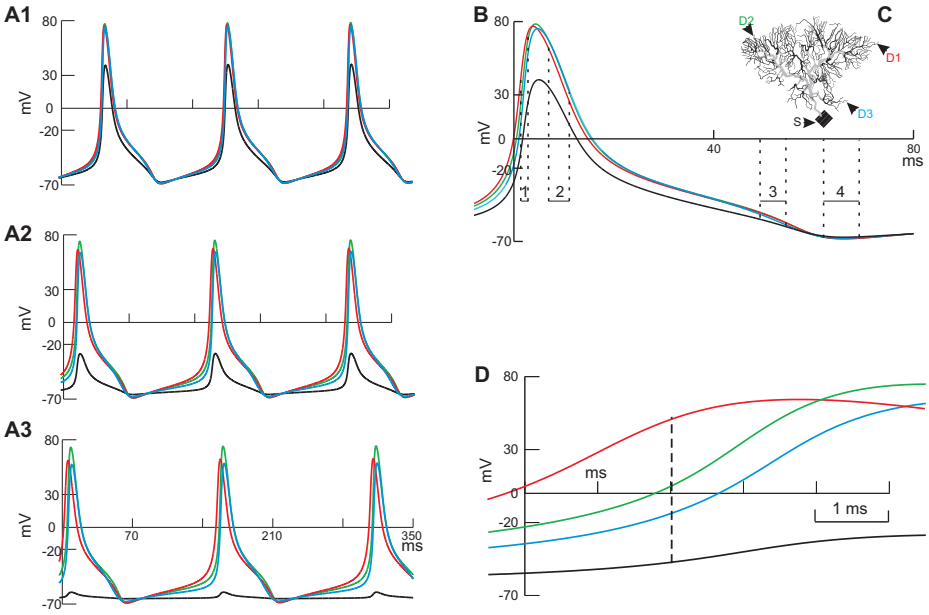

Figure 5: Oscillatory potentials generated by the Purkinje cell receiving distributed tonic synaptic excitation. **A1**: Regular auto-oscillations computed with $G_m = 677.25$ $\mu S/cm^2$ and recorded from the soma (black trace) and 3 dendritic sites (red, green and blue superimposed traces). **B**: A single expanded oscillatory cycle extracted from A1 to show the phase-shifted recordings from the soma S (in black) and from 3 dendritic sites D1 (in red), D2 (in green), and D3 (in blue) localized on the 3D arborization shown in **C**. The four horizontal black bars and vertical dotted lines labelled 1 to 4 (under the potentials) indicate the phases of the oscillatory potential during which snapshots were collected and are depicted in Fig. 6. **A2**: Same recordings as in A1 but computed with $G_m = 6{,}772.5$ $\mu S/cm^2$ to show the differences in amplitudes and shift in time as compared to A1. **A3**: Same recordings as in A1 but computed with $G_m = 67{,}725$ $\mu S/cm^2$. **D**: A single oscillatory cycle extracted from A2 with an expanded time scale to show better the differences in time and amplitude (dotted lines) between the recordings. Abscissae: time in ms. Note the different time-scales. Ordinates: voltage in mV.

Figure 5 shows the simulated membrane potentials computed with 3 different values

of G_m. The wide range within which the model operated effectively for producing slow oscillations was used to test its robustness. In A1 ($G_m = 677.25\ \mu S/cm^2$), three oscillations were recorded from the soma (S) and from 3 different dendritic sites (sites S and D1, D2, D3 shown on the 3D representation of the arborization in Figure 5 C). The four recordings were of different amplitudes, of slightly different shapes and each occurred with a shift in time. One example of a single oscillation extracted from A1 is shown in Fig. 5 B with an expanded time scale to illustrate the shift in time. The first potential to be recorded was from D1 (red trace) and had a peak amplitude of $76.6mV$. The second potential was recorded from D2 (green trace) with the highest amplitude of $79.0mV$ followed by the potential from D3 (blue trace) of $75mV$ in amplitude. The delayed potential recorded from the soma (black trace) had a peak amplitude of $40mV$. In Fig. 5 A2 ($G_m = 6{,}772.5\ \mu S/cm^2$), the dendritic recordings were similar to those in A1 but with a slightly larger shift in time while the somatic recording displayed a much smaller amplitude reaching -40 mV. The difference in time and amplitude between the four recorded potentials (extracted from one oscillation in A2) was best illustrated in Fig. 5 D when observed with an expanded time scale at the start of the rising phase of the oscillation. The main result was that the recording D1 preceded D2 and D3 by several milliseconds. The difference in amplitudes between the potentials recorded at given sites (S, D1, D2, D3) of the dendritic arborization and at a given moment of time (dashed lines)of the oscillation were, for example, as large as around 100 mV between D1 and soma (Fig. 5 D). Figure 5 A3 ($G_m = 67{,}725\ \mu S/cm^2$) shows a larger difference in amplitude between dendritic and somatic recordings. There is also a difference in amplitude and a larger shift in time with respect to the values observed in A1 and A2. The demonstration that the oscillatory potentials were ordered in time was a new and important finding that facilitated further the understanding of the dynamics of the membrane potentials in the dendritic field observed in space.

Dynamics of the spatial reconfiguration of membrane potentials during an oscillatory potential.

By taking a video of the dendritic maps of the membrane potentials during a single oscillation revealed that the functional geometry of the arborization was not static but changed in space in the course of the oscillation. Successive snapshots of the maps extracted from the video were taken during the 4 phases 1, 2, 3 and 4 of the oscillatory cycle indicated in Fig. 5 B and are illustrated in Fig. 6. The sequence in which the dendritic domains changed their consecutive colours allowed to identify the sequence of changes in the membrane potential and derive the phase relationships of the events at these domains. This proper procedure allowed to demonstrate the split of the dendritic arborization into domains of different voltage transients. Noteworthy these domains were like those identified in the passive configuration in the steady state (Fig. 3 d).

During the first phase of the cycle starting at the beginning of the rising phase of the potential (t = 1.2 ms), almost the entire dendritic arborization was set at a potential between +25.0 to +31.67 mV except a tiny North-East domain between +31.67 to +38.33 mV (Fig. 6, column 1). The following snapshots in the column showed that the shift to higher values involved first the North-East domain (+38.33 mV). Then the arborization was split into successive dendritic domains with low to high values of voltages characterized by their ordered spatial sequence. The North-East domain reached the highest voltage (+58.33 to +65.00 mV) first (sixth snapshot in column 1). A state of fully depolarized dendritic arborization (Fig. 6, column 2) was reached just before the beginning of phase 2 (indicated in Fig. 5 B) corresponding to the start of the repolarizing phase of the potential (t = 6.8 ms). At that given moment, the soma was depolarized between +31.67 and +38.33 mV. On the way back to repolarization (column 2), the split between domains occurred again in an inverse order to reach voltages between +38.33 and +25 mV at the end of column 2. At the beginning of phase 3 (Fig.

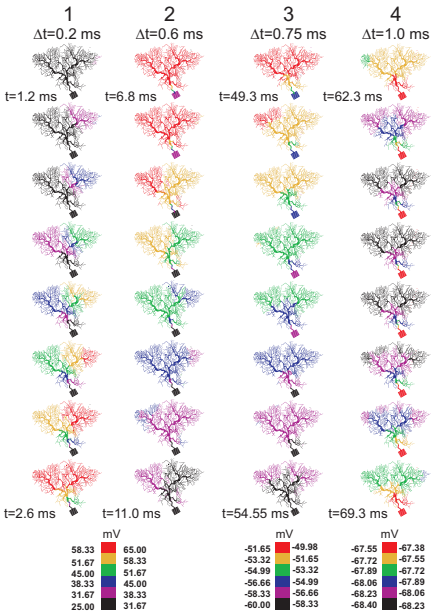

Figure 6: Dynamics of the electrical states of the membrane of the Purkinje cell arborization. Snapshots of the dendritic maps of the membrane potentials taken during phase 1 to 4 of the oscillatory cycle shown under the potential in Fig. 5 B. Column 1 to 4 shows eight snapshots taken with equal time step Δt from top to bottom. Column 1 corresponds to the rising phase of the potential, starts at $t = 1.2ms$, snapshots taken every $0.2ms$ and ends at $t = 2.6ms$. Column 2 corresponds to the falling phase of the plateau potential, starts at $t = 6.8ms$, snapshots taken every $0.6ms$ and ends at $t = 11.0ms$. Column 3 and 4 correspond to increasing ($\Delta t = 0.75ms$) and decreasing ($\Delta t = 1.0ms$) inter-plateau hyperpolarizations starting at $t = 49.3ms$ and $62.3ms$ and ending at $t = 54.55ms$ and $t = 69.3ms$ respectively. Membrane potential is colour-coded in mV: from 25.00 to 65.00 mV for columns 1 and 2, from -49.98 to 60.00 mV for column 3 and from -67.38 to -68.40 mV for column 4. Note that the different scales of colour used for the different rows express different scales of voltages.

6, column 3, t = 49.3 ms), the arborization was hyperpolarized between -49.98 and -51.65 mV, except some small domains near the soma. During phase 3, the arborization was again orderly divided into domains showing potentials between -51,65 and -60.00 mV with regional differences of some tenths of mV. During phase 4, (Fig. 6, column 4, t = 62.3 ms), successive dendritic domains were still changing towards hyperpolarization but the differences between dendritic parts was reduced to only 1 mV (-67.55 to -68.23 mV). Then, a new cycle started with the same successive spatial patterns of splits (not shown). The turnover of the regional different polarizations of the dendritic membrane lasted the duration of one cycle. One important finding was the fact that the same dendritic sector in the arborization displayed a difference in voltage as high as about $130mV$ during a single oscillation (see Fig. 5 D). For example, the North-East domain which displayed +58 to +65 mV at the beginning of the falling phase of the oscillation (row 2), was hyperpolarized to -68 mV at the end of the oscillatory cycle (row 4). The dynamics of the spatio-temporal reconfiguration characterizing the oscillations is best illustrated by the video provided in the supplementary material.

DISCUSSION

This work is based on the assumption that geometry of the dendritic arborization of the Purkinje neuron has a significant impact on its main electrical characteristics which determine its electrophysiological patterning.

Numerous compartmental models have combined morphological and electrophysiological data obtained from different types of cells (58; 10; 59; 42; 9) and from Purkinje neurons (51; 11; 12; 19; 53; 63; 48) to study the biophysical parameters characteriz-

ing these neurons by direct fits of the transient responses recorded from it. The aim was to replicate the results obtained in electrophysiological experiments *in vivo* or *in vitro*. Thus, these studies were orientated towards single or two-sites recordings. This preference for digging out reliable estimates of biophysical parameters provided important results and has proved very useful. However, the models were often reduced to two compartments considered to be sufficient for all important predictions. The two compartments represented only proximal and distal parts of the whole tree, allowing to explore the distal-to-proximal electrical relations along dendrites while the electrical relations between different dendritic paths were neglected.

Our simulation of the Purkinje neurons complements previous modelling studies and differs in several respects. First, the electrotonic structure is used as a tool for tracking metrical asymmetry of the dendritic paths. Although indirect, it is a good indicator for revealing this crucial morphological feature in the tree and its electrical consequences. Second, electrical relations between any dendritic sites are assessed and result in a full description of the electrical states of all sites in the membrane. Third, if transients are omitted in our model, it is because they prevent the observation of what happens locally and simultaneously in most locations of the whole tree. Finally, the active configuration performed with voltage-dependent conductances incorporated in the dendritic membrane provides spatial data on the electrical behaviour of the different sub-trees during slow oscillatory potentials when the exchange of current between dendritic sites provides dynamics of temporal patterns.

The electrotonic structure of the arborization

The simulation of the **passive** dendrite relies on the complete reconstruction of the cell at high spatial resolution and provides a conventional reference for the layout of the electrical patterns which can be traced further in non-linear configurations.

The spatial profiles of somatofugal voltages are equivalent to the somatopetal current transfer effectiveness (4; 8; 35). This 1D representation of the tree is the only indirect tool allowing to explore the effects of local geometry on the current transfer effectiveness along each dendritic paths. By comparing the spatial patterns along the different paths, we show that the electrical differences between the profiles can only occur because of differences in length and diameters along the dendritic paths in the whole tree i.e. the **metrical asymmetry** between daughter paths. Unfortunately, no mathematical tools are currently available to quantify the metrical asymmetry whereas the topological asymmetry indices are not applicable (54; 61; 62). Nevertheless, the effect of asymmetry can be observed in the 1D representation of the current transfer effectiveness profiles in which the presence of different bundles is displayed. These bundles are the signature of asymmetry. We conclude that among specific geometrical features of the dendritic branches, metrical asymmetry of the branches results in a spatial functional partition of the tree.

These partitions are observed in the six neurons analyzed in this work but with slight differences that are geometrical in origin as morphology is the only variable parameter between the neurons. One possible explanation for the difference between the trees in their spatial partitions is found in the morphometrical analysis of the terminal segments which show unexpectedly large diameters in all cells but one (P1). As already noted by (53), the measurement of diameters may be subject to considerable error, particularly for the finest dendrites. This difficulty of measurements cause differences between morphological data acquisitions that in turn bear on the simulation results (24; 30). Large tip diameters correspond to thick ends and mean greater leak through the membrane of terminal segments. Thus, the leak decreases the charge transfer effectiveness as less current flows to the soma and more current flows out through the leak. Thus, the direction and quantity of current is conditioned by the geometry of the branchlets which in turn

affect the features of the spatial partitions. This finding constitutes one supplementary argument supporting the pivotal role of geometry in determining the electrical states of the dendritic membrane.

The active model

The simulation of the **active** dendrite when the cell generates typical slow oscillatory potentials, provides dynamics of temporal transient patterns. During a single oscillation, a differential distribution of membrane potentials in the arborization characterized different dendritic domains of different sizes, tracing the same regional organization observed in the passive model. For example, the North-East part of the dendritic field that is identified in the passive configuration as showing the lowest efficiency exhibits the highest membrane potentials at the beginning of the rising phase of the oscillation. Then it is the first domain to reach the highest membrane potential ($65.00mV$) when the single-site recording D1 reaches also the peak amplitude of the oscillatory potential. The two other domains where the recordings D2 and D3 are located, are shifted in time with a small delay before reaching the peak amplitude of the oscillatory potential and simultaneously, these two domains are highly depolarized but clearly separated both in space and time. The explanation for the observed shift in time is that D1, located in a domain with small diameters and great asymmetry, displays a greater input resistance on which the inward currents produce greater voltage drop as compared to D2 and D3. If a smaller proportion of charges is transferred to the soma from D1, a greater proportion must be spent locally to build up the charge on the membrane capacitor at the entry of the current. The charges deposited on the local capacitor generate depolarization and hyperpolarization depending on the sign of the charge. As a consequence, the same depolarization is built up faster in D1 as compared to the more effective sites D2 and D3 which loose their charges due to a more effective transfer to the soma.

The striking finding that emerges from these new results is that metrical asymmetry of the arborization during oscillations induces the sector-like spatial organization of the transient electrical states with distinct sectors similar to those observed in the passive electrotonic structure in the steady state. Namely, the dendritic domains which differ in their steady-state passive transfer properties become different in their electrical states during the transients. Electrical oscillations in those domains are ordered in phase. They are advanced in phase in the regions with lower effectiveness of the passive transfer of somatopetal current. They are delayed in phase in the region with higher effectiveness. The comparison of compartmentalizations of the dendritic arborization in the passive configuration and during slow oscillations strongly suggests that the branching metrical asymmetry explains such compartmentalizations.

The spatial dynamic electrical image of the whole operating tree is a new finding. It may be related to other published materials in which similar spatio-temporal picture can be observed. For example, (11), in comments of their Figure 10 B and C showing images of membrane potential distribution and calcium concentration during a somatic action potential and a dendritic spike, noticed that the dendritic spikes did not fire synchronously in all regions of the dendritic tree trying to originate in an electrotonically most distant branch from the soma and spread as a wave to a less distant part of the dendrite. It is highly probable that the authors show fragmentarily spatio-temporal pictures similar to those described here. Notably, the dendritic sub-tree where the highest value of membrane potential and calcium concentration are observed by the authors corresponds to the domain identified in our results as being the least effective in charge transfer to the soma.

Physiological implications

The discharge patterns of the Purkinje neuron (27) are currently recorded from the soma, the stem dendrite or from multiple dendritic sites and are interpreted in single-site somatocentric terms: initiation site at the trigger zone, orthodromic propagation along the axon, back-invasion into the dendrite, dendritic spikes, boosting of distal EPSPs. (11; 12; 56; 60; 19; 53; 63). Taken together, these studies provide important information about dendritic excitability, modulation of synaptic potentials, efficacy of backpropagating action potentials and non-uniformities in the membrane properties of the Purkinje cell.

Our findings complements these results in drawing attention to some missing pieces which may be of importance for understanding further the rules that govern dendritic processing in the Purkinje neuron. By introducing the dynamics of the dendritic space, we reveal a robust geometry-induced functional spatial fragmentation of the Purkinje cell arborization. A new unreported characteristic of the Purkinje cell dendrite shown in this study is the strong relation between the spatial steady transfer pattern and the spatio-temporal pattern of the oscillatory potentials. Our data extend to existing results demonstrating the impact of dendritic geometry on the electrical behaviour of the neuron (7; 35; 33; 34; 32). Most important is the observation of the continuous spatial electrical reconfiguration that occurs in a phase-ordered manner over the dendritic membrane during oscillations. This finding indicates that the membrane of the dendritic field as a whole is not a static element but changes continuously during oscillations in terms of domains of different charge transfer efficiency.

The present results open the question of the pre- and post-synaptic scenario when the Purkinje neuron is bombarded by the synaptic systems of climbing fibres and parallel fibres. The great majority of the studies focus upon the synaptic connection. The presynaptic factors as well as the postsynaptic membrane receptors are extensively analyzed

(46; 1). Meanwhile the role of the electrical states of the dendritic membrane per se, as the receiving target, is rarely addressed. If the results of our simulations are correctly interpreted, it can be suggested that the synaptic afferent systems to single Purkinje neurons meet different domains of the dendritic membrane which display different transfer efficiencies at a given time. Our results show spatial dendritic sectors separated by a difference in voltage as high as about 100 mV during a single oscillation (see Fig. 6). As a consequence, these functional dendritic sectors which are alternatively turned on and off during a cycle may be a plastic device for selecting synaptic inputs.

One example illustrates well our speculation. Data published recently by (26) on undetected synapses between granule cells and Purkinje cells suggest that a large fraction of parallel fiber synapses do not generate electrical responses in the Purkinje cell. Several hypotheses are proposed to explain this fact, either action potential in parallel fiber fails to reach distant synapses, or connections have low release probabilities or some synapses have no functional postsynaptic AMPA receptors. An additional or optional explanation which is not exclusive can be suggested. The parallel fibers bombarding the Purkinje dendritic membrane meet some parts of the dendritic field which are, at that given moment, not effective in transmitting current to the soma. Thus, the synapse is silent not because of a presynaptic scenario, but because the dendritic branches that are contacted are functionally disconnected from the soma. The electrical dynamics of the dendritic field endow the neuron with the ability to select its own inputs according to the context in which the synapse operates. If one consider that adjacent parallel fibres (and therefore granule cells) contact adjacent dendritic spines, and that relatively large individual domains of the dendritic space show the same charge transfer effectiveness, one may speculate that, because of its dendritic geometry, the Purkinje cell is capable of selecting one or another bundle of the 200,000 parallel fibres to be efficient.

The selection of afferent inputs by the Purkinje neuron is compatible with the reg-

ulation of motor learning, particularly of the fine movements. The problem of silent synapses is reviewed in several recent articles (43; 44; 2; 25) in which pre- and postsynaptic mechanisms are discussed often in the context of LTP, cortical plasticity, learning and memory (52; 55; 49). Additional to the numerous hypothesis suggesting mechanisms that may create silent synapses and lead to their switching to an active state, the electrical spatial dynamics of the dendritic field may as well be an optional explanation.

The experimental verification of our spatial hypothesis requires complementing the conventional electrophysiological approach with new tools that provide a full description of the local transmembrane potential in the dendritic membrane over large regions of the arborization (17; 57; 69; 13; 47). This can be performed by cellular imaging with voltage-sensitive dyes acting as a sensor of local electrical field in the membrane. The predictions of our simulations imply that space and time are necessarily bound together in a new language to describe the firing patterns of the neuron.

Acknowledgements: We are grateful to Dr. Paul Gogan for criticizing our manuscript, to Dr. D. Rusakov for his helpful comments, to Valery Kukushka for providing simulation tools and to Michelle Morel and Michèle Elléon for their technical help. We thank Dr. John Lagnado for scrutinizing the English language. This work was supported by DNIPRO from French Ministry of Foreign Affairs and Ministry of Education and Science of Ukraine, by ESPCI, Mairie de Paris (visiting Professor grants to S.M.K.) and Université de la Méditerrannée (visiting Professor grants to S.M.K. and I.B.K.). The authors thank Mr. M. Pierre, Centre de Formation et de Coopération franco-ukrainien in Kiev for his efficiency.

Supplementary material The online version of this paper (http://www.neurones.espci.fr/) contains supplementary material entitled *"Video of P1 arborization during oscillatory potentials: the spatial dynamics of the activity".*

References

[1] H. L. Atwood and S. Karunanithi. Diversification of synaptic strength: presynaptic elements. *Nature Rev. Neurosci.*, 3:497–516, 2002.

[2] H. L Atwood and J. M. Wojtowicz. Silent synapses in neural plasticity: current evidence. *Learning and Memory*, 6:542–571, 1999.

[3] A. Aubry, C. Batini, J. M. Billard, R. T. Kado, and P. Morain. Tetrodotoxin induced calcium spikes: in vitro and in vivo studies of normal and deafferented Purkinje cells. *Exp. Brain Res.*, 84:297–302, 1991.

[4] J. N. Barrett and W. E. Crill. Influence of dendritic location and membrane properties on the effectiveness of synapses on cat motoneurones. *J. Physiol.(London)*, 239:325–345, 1974.

[5] C. Batini and R. T. Kado. Analyse quantitative de l'activit spontanée et évoquée des cellules de Purkinje. *J. Physiol. Paris*, 59:209–210, 1967.

[6] H. Bras, P. Gogan, and S. Tyč-Dumont. The dendrites of single brain-stem motoneurons intracellularly labelled with horseradish peroxidase in the cat. Morphological and electrical differences. *Neuroscience*, 22:947–970, 1987.

[7] H. Bras, S. Korogod, Y. Driencourt, P. Gogan, and S. Tyč-Dumont. Stochastic geometry and electrotonic architecture of dendritic arborization of a brain-stem motoneuron. *Eur. J. Neurosci.*, 5:1405–1493, 1993.

[8] N. T. Carnevale and D. Johnston. Electrophysiological characterization of remote chemical synapses. *J Neurophysiol.*, 47:606 621, 1982.

[9] R. A. Chitwood, A. Hubbard, and D. B. Jaffe. Passive electrotonic properties of rat hippocampal CA3 interneurones. *J. Physiol.*, 515:743–756, 1999.

[10] J. D. Clements and S. J. Redman. Cable properties of cat spinal motoneurones measured by combining voltage clamp, current clamp and intracellular staining. *J. Physiol*, 409:63–87, 1989.

[11] E. De Schutter and J. Bower. An active membrane model of the cerebellar Purkinje cell 1. simulation of current-clamps in slice. *J Neurophysiol.*, 71:375–400, 1994a.

[12] E. De Schutter and J. Bower. An active membrane model of the cerebellar Purkinje cell 2. simulation of synaptic responses. *J Neurophysiol.*, 71:401–419, 1994b.

[13] M. Djurisic, S. Antic, W. R. Chen, and D. Zecevic. Voltage imaging from dendrites of mitral cells: EPSP attenuation and spike trigger zones. *J. Neurosci.*, 24:6703–6714, 2004.

[14] J. C. Eccles, M. Ito, and J. Szentágothai, editors. *The cerebellum as a neuronal machine*. Springer-Verlag, Berlin, 1967.

[15] C. A. Fox and J. W. Barnard. A quantitative study of the Purkinje cell dendritic branchlets and their relationship to afferent fibers. *J. Anat.(London)*, 91:299–313, 1957.

[16] E. M. Glaser and H. Van der Loos. A semiautomatic computer microscope for the analysis of neuronal morphology. *IEEE Trans. Biomed. Eng.*, 12:22–31, 1965.

[17] P. Gogan, I. Schmidel-Jakob, Y. Chitti, and S. Tyč-Dumont. Fluorescence imaging of local membrane electric fields during the excitation of single neurons in culture. *Biophys. J.*, 69:299–310, 1995.

[18] J. Hamori and J. Szentágothai. The "crossing over synapse". an electronmicroscope study of the molecular layer in the cerebellar cortex. *Acta Biol. Acad. Sci. Hung.*, 15:95–117, 1964.

[19] M. Häusser, N. Spruston, and G. J. Stuart. Diversity and dynamics of dendritic signaling. *Science*, 290:739–744, 2000.

[20] M. L. Hines and N. T. Carnevale. Neuron - a tool for neuroscientists. *Neuroscientist*, 7:123–135, 2001.

[21] M. L. Hines. Neuron - a program for stimulation of nerve equations with branching geometries. *Int. J. Biomed. Comput.*, 24:25–68, 1989.

[22] T. Hirano and S. Hagiwara. Kinetics and distribution of voltage-gated Ca, Na and K channels on the somata of rat cerebellar Purkinje cells. *Pflug. Archiv-Euro. J. Physiol.*, 413:463–469, 1989.

[23] T. Hollingworth and M. Berry. Network analysis of dendritic fields of pyramidal cells in neocortex and Purkinje cells in the cerebellum of the rat. *Phys. R. Soc. Ser. B*, 270:227–264, 1975.

[24] G. Horcholle-Bossavit, P. Gogan, Y. Ivanov, S. Korogod, and S. Tyč-Dumont. The problem of morphological noise in reconstructed dendritic arborizations. *J. Neurosci. Meth.*, 95:83–93, 2000.

[25] J. T. Isaac. Postsynaptic silent synapses: evidence and mechanisms. *Neuropharmacol.*, 45:450–460, 2003.

[26] P. Isope and B. Barbour. Properties of unitary granule cell to → Purkinje cell in adult rat cerebellar slices. *J. Neurosci.*, 15:9668–9678, 2002.

[27] M. Ito, editor. *The cerebellum and neural control*. Raven Press, New-York, 1984.

[28] M. Ito. Long term depression: characterization, signal transduction and functional roles. *Physiol. Rev.*, 81:1143–1195, 2001.

[29] R. T. Kado, P. Morain, and C. Batini. Cerebellar Purkinje cell: membrane property changes on partial deafferentation. In J. Physiol. (Paris), editor, *Mechanisms underlying long lasting changes in neuronal properties: fact and perspectives.*, volume 83, pages 172–180, Paris, 1989. Masson.

[30] A. V. Kaspirzhny, P. Gogan, G. Horcholle-Bossavit, and S. Tyč-Dumont. Neuronal morphology data bases: morphological noise and assesment of data quality. *Network: Comput. Neural Syst.*, 13:357–380, 2002.

[31] S. M. Korogod, H. Bras, V. N. Sarana, P. Gogan, and S. Tyč-Dumont. Electrotonic clusters in the dendritic arborisation of abducens motoneurons in the rat. *Euro. J. Neurosci.*, 6:1517–1527, 1994.

[32] S. M. Korogod, I. B. Kulagina, V. I. Kukushka, P. Gogan, and S. Tyč-Dumont. Spatial reconfiguration of charge transfer effectiveness in active bistable dendritic arborizations. *Europ. J. Neurosci.*, 16:2260–2270, 2002.

[33] S. M. Korogod and I. B. Kulagina. Geometry-induced features of current transfer in neuronal dendrites with tonically activated conductances. *Biol. Cybern.*, 79:231–240, 1998.

[34] S. M. Korogod, I. Kulagina, G. Horcholle-Bossavit, P. Gogan, and S. Tyč-Dumont. Activity-dependent reconfiguration of the effective dendritic field of motoneurons. *J. Comp. Neurol.*, 442:18–34, 2000.

[35] S. M. Korogod. Electro-geometrical coupling in non-uniform branching dendrites. *Biol. Cybern.*, 74:85–93, 1996.

[36] R. Latorre, A. Oberhauser, P. Labarca, and O. Alvarez. Kinetics of calcium-activated potassium channels. *Ann. Rev. Physiol.*, 81:385–399, 1989.

[37] R. Llinás and D. E. Hillman. Physiological and morphological organization of the cerebellar circuits in various vertebrates. In R. Llinás, editor, *Neurobiology of cerebellar evolution and development*, page 931, Washington, 1969. American Medical Ass.

[38] R. Llinás, M. Sugimori, B. Lin, and B. J. Cherksey. Blocking and isolation of a calcium-channel from neurons in mammals and cephalopods utilzing a toxin fraction (FTX) from funnel-web spider poison. *Proc. Nat. Acad. Sci. USA*, 86:1689–1693, 1989.

[39] R. Llinás and M. Sugimori. Electrophysiological properties of *in vitro* Purkinje cell somata in mammalian cerebellar slices. *J. Physiol.*, 305:171–195, 1980a.

[40] R. Llinás and M. Sugimori. Electrophysiological properties of *in vitro* Purkinje cell dendrites in mammalian cerebellar slices. *J. Physiol.*, 305:197–213, 1980b.

[41] Y. Loewenstein, S. Mahon, Paul Chadderton, K. Kitamura, H. Sompolinsky, Y. Yarom, and M. Häusser. Bistability of cerebellar Purkinje cells modulated by sensory stimulation. *Nature Neuroscience*, 8:202–, 2005.

[42] Z. F. Mainen, N. T. Carnevale, A. M. Zador, B. J. Claiborne, and T. H. Brown. Electrotonic architecture of hippocampal ca1 pyramidal neurons based on three-dimensional reconstructions. *J. Neurophysiol.*, 76:1904–1923, 1996.

[43] R. Malenka. Silent synapses in the hippocampus and cortex. In D. S. Faber, H. Korn, S. J. Redman, S. M. Thomson, and J. S. Altman, editors, *Central synapses: Quantal mechanisms and plasticity*, pages 207–214, Strasbourg, France, 1998. Human Frontier Science Program.

[44] R. Malinow. Silent synapses in three forms of central plasticity. In D. S. Faber, H. Korn, S. J. Redman, S. M. Thomson, and J. S. Altman, editors, *Central synapses:*

Quantal mechanisms and plasticity, pages 226–234, Strasbourg, France, 1998. Human Frontier Science Program.

[45] R. C. Miall, J. G. Keating, M. Malkmus, and W. T. Thach. Simple spike activity predicts occurence of complex spikes in cerebellar Purkinje cells. *Nature Neuroscience*, 1:13–15, 1998.

[46] J. Midtgaard. Processing of information from different sources: spatial synaptic integration in the dendrite of vertebrate CNS neurons. *Trends Neurosci.*, 17:166–173, 1994.

[47] B. A. Milojkovic, M. S. Radojicic, and S. D. Antic. A strict correlation between dendritic and somatic plateau potential depolarizations in the rat prefontal cortex pyramidal neurons. *J. Neurosci.*, 25:3940–3951, 2005.

[48] T. Miyasho, H. Takagi, H. Suzuki, M. Watanabe, S. Inoue, Y. Kudo, and H. Miyakawa. Low-threshold potassium channels and a low-threshold calcium channel regulate Ca^{2+} spike firing in the dendrites of cerebellar Purkinje neurons: a modeling study. *Brain Res.*, 891:106–115, 2001.

[49] A. Pascual-Leone, A. Amedi, F. Fregni, and L. B. Merabet. The plastic human brain cortex. *Annu. Rev. Neurosci.*, 28:377–401, 2005.

[50] A. Pellionisz and R. R. Llinás. A computer model of cerebellar Purkinje cells. *Neuroscience*, 2:37–48, 1977.

[51] M. Rapp, Y. Segev, and Y. Yarom. Physiology, morphology and detailed passive models of guinea-pig cerebellar Purkinje cells. *J. Physiol.*, 474:101–108, 1994.

[52] M-S. Rioult-Pedotti and J. P. Donoghue. The nature and mechanisms of plasticity. In S. Boniface and U. Ziemann, editors, *Plasticity in the human nervous system.*

Investigation with transcranial magnetic stimulation., pages 1–25, Cambridge, 2003. Cambridge University Press.

[53] A. Roth and M. Häusser. Compartmental models of rat cerebellar Purkinje cells based on simultaneous somatic and dendritic patch-clamp recordings. *J. Physiol.*, 535:445–472, 2001.

[54] M. Sadler and M. Berry. Link-vertex analysis of Purkinje cell dendritic trees from the murine cerebellum. *Brain Res.*, 22:130–146, 1988.

[55] J. N. Sanes. Neocortical mechanisms in motor learning;. *Curr. Opin. Neurobiol.*, 13:225–231, 2003.

[56] F. Santamaria, D. Jaeger, E. De Schutter, and J. M. Bower. Modulatory effects of parallel fiber and molecular layer interneuron synaptic activity on Purkinje cell responses to ascending segment input: a modeling study. *J. Comput. Neurosci.*, 13:217–235, 2002.

[57] L.P. Savtchenko, P. Gogan, S. M. Korogod, and S. Tyč-Dumont. Imaging stochastic spatial variability of active channel clusters during excitation of single neurons. *Neurosci. Res.*, 39:431–446, 2001.

[58] D. P. Shelton. Membrane resistivity estimated for the Purkinje neuron by means of a passive computer model. *Neuroscience*, 14:111–131, 1985.

[59] N. Spruston and D. Johnston. Perforated patch-clamp analysis of the passive membrane properties of three classes of hippocampal neurons. *J Neurophysiol.*, 67:508–529, 1992.

[60] G. J. Stuart and M. Häusser. Initiation and spread of sodium action potentials in cerebellar Purkinje cells. *Neuron*, 13:703–712, 1994.

[61] J. Van Pelt, H. B. M. Uylings, R. W. H.. Verwer, R. J. Pentney, and M. J. Woldenberg. Tree symmetry: a sensitive and practical measure for binary topological trees. *Bull. Math. Biol.*, 54:759–784, 1992.

[62] R. W. H. Verwer, J. Van Pelt, and H. B. M.. Uylings. An introduction to topological analysis of neurones. In M. G. Stewart, editor, *Quantitative Methods in Neuroanatomy*, pages 295–323, New-York, 1992. John Wiley and sons.

[63] P. Vetter, A. Roth, and M. Häusser. Propagation of action potentials in dendrites depends on dendritic geometry. *J. Neurophysiol.*, 85:926–937, 2001.

[64] R. Vigot and C. Batini. $GABA_B$ receptor activation in Purkinje cells in cerebellar slices. *Neurosci. Res.*, 29:151–160, 1997.

[65] R. Vigot and C. Batini. Purkinje cell inhibitory responses to 3-APPA (3-aminopropylphosphinic acid) in rat cerebellar slices. *Neurosci. Res.*, 34:141–147, 1999.

[66] D. F. Wann, T. A. Woosley, M. L. Dierker, and W. M. Cowan. An on-line computer system for the semiautomatic analysis of golgi-impregnated neurons. *IEEE Trans. Biomed. Eng.*, 20:233–247, 1973.

[67] S. R. Williams, G. R. Christensen, J. G. Stuart, and M. Häusser. Membrane potential bistability is controlled by hyperpolarization-activated current ih in rat cerebellar Purkinje neurons in vitro. *J. Physiol.*, 539:469–483, 2002.

[68] W. Yamada, C. Koch, and P. Adams. Multiple channels and calcium dynamics. In C. Koch and I. Segev, editors, *Methods in Neuronal Modeling: From synapses to networks.*, pages 97–234, Cambridge, 1989. MIT Press.

[69] D. Zecevic. Multiple spike-initiation zones in single neurons revealed by voltage-sensitive dyes. *Nature*, 381:322–325, 1996.